A Simple Impedance Reshaping Method for Stability Enhancement of Grid-Following Inverter Under Weak Grid

Huang, Liang; Wu, Chao; Zhou, Dao; Blaabjerg, Frede

Published in:
2021 IEEE 12th International Symposium on Power Electronics for Distributed Generation Systems (PEDG)

DOI (link to publication from Publisher):
10.1109/PEDG51384.2021.9494181

Publication date:
2021

Document Version
Accepted author manuscript, peer reviewed version

A Simple Impedance Reshaping Method for Stability Enhancement of Grid-Following Inverter Under Weak Grid

Liang Huang
Department of Energy Technology
Aalborg University
Aalborg, Denmark
lihu@et.aau.dk

Chao Wu
Department of Energy Technology
Aalborg University
Aalborg, Denmark
cwu@et.aau.dk

Dao Zhou
Department of Energy Technology
Aalborg University
Aalborg, Denmark
zda@et.aau.dk

Frede Blaabjerg
Department of Energy Technology
Aalborg University
Aalborg, Denmark
fbl@et.aau.dk

***Abstract*—The conventional vector current control (VCC) scheme has been widely used in the grid-connected inverter systems. However, it suffers from power limitation problems under weak grid conditions. This paper reveals that the dynamic effect of the phase-locked loop (PLL) is the main reason for destabilizing the small-signal stability of the grid-following inverter. The positive feedback introduced by the PLL can be observed from the small-signal control structure. Reshaping the converter output impedance can counteract the positive feedback and reduce the negative resistance in the impedance model. A novel impedance reshaping method is proposed in this paper, which can enhance the small-signal stability and extend the stability range of the system. Simulation results verify the effectiveness of the proposed method.**

Keywords—grid-following inverter, vector current control, small-signal model, stability enhancement, weak grid

I. INTRODUCTION

As the penetration rate of wind generation increases, the power grid connected to the renewable energy generation is weaker than before due to the larger transmission impedance and smaller short-circuit ratio (SCR) [1], which leads to power limitation issues [2]. Two aspects should be considered for such power limitation issues. When the mathematical model of the system is established based on the steady-state equations, the power limit only depends on the parameters of the grid impedance. This power limit is called the static power limit [3], which can be obtained by using phasor analysis. When the mathematical model of the system is established based on the dynamic equations, the control stability issue can be included. Thus, another power limit can be obtained by using small-signal stability analysis, which is called the small-signal stability limit [3]. This small-signal stability limit mainly depends on the control scheme, so that it can be changed by choosing different control schemes. Hence, how to modify the control scheme to increase the small-signal stability range becomes a hot topic [4].

Although a lot of grid-forming control methods based on the power synchronization have been presented in [5], the conventional grid-following vector current control (VCC) method based on phase-locked loop (PLL) is still a mainstream method for the grid-connected inverter in wind generation systems. It attracts significant attention to reveal the instability mechanism and enhance the stability of inverters under weak AC grid conditions [6], [7].

Reference [8] shows that there is an equivalent *q*-*q* negative resistance in the small-signal impedance model which is introduced by the PLL. Since the *q*-*q* negative resistance causes positive feedback in the control loop [9], [10], it is a major destabilizing factor. To solve this problem, [9] proposes an impedance reshaping method based on the precondition of unity power factor (UPF). However, under weak grid conditions, the reactive power is necessary to support the voltage at the point of common coupling (PCC), so the UPF condition is usually not satisfied. Moreover, [10] proposes an impedance reshaping method based on a symmetrical PLL. However, the symmetrical PLL is more complicated than the classical PLL, and there are some control challenges when the grid voltage amplitude changes. Additionally, [11] proposes a bandpass filter method to weaken the impact of the negative resistance. Reference [12] proposes a pre-filter method in the PLL to reduce this negative resistance impact. However, the specific enlarged quantity of the stability range is not revealed in these existing research.

Differently, this paper proposes a novel impedance reshaping method based on the classical PLL, which is easy to implement. Besides, the small-signal stability boundary of the proposed method can be estimated by using the Generalized Nyquist Criterion (GNC), so that the small-signal stability range can be evaluated quantitatively.

The rest of this paper is organized as follows. Section II introduces the configuration of the grid-following inverter and its small-signal impedance model. Section III analyzes the proposed impedance reshaping method and its implementation. Then, the simulation parameters and results are shown in Section IV. Finally, this paper is concluded in Section V.

II. MODELING OF GRID-FOLLOWING INVERTER

A. Configuration of Grid-Following Inverter

A schematic diagram of the classical VCC grid-following inverter connected to a weak grid is shown in Fig. 1.

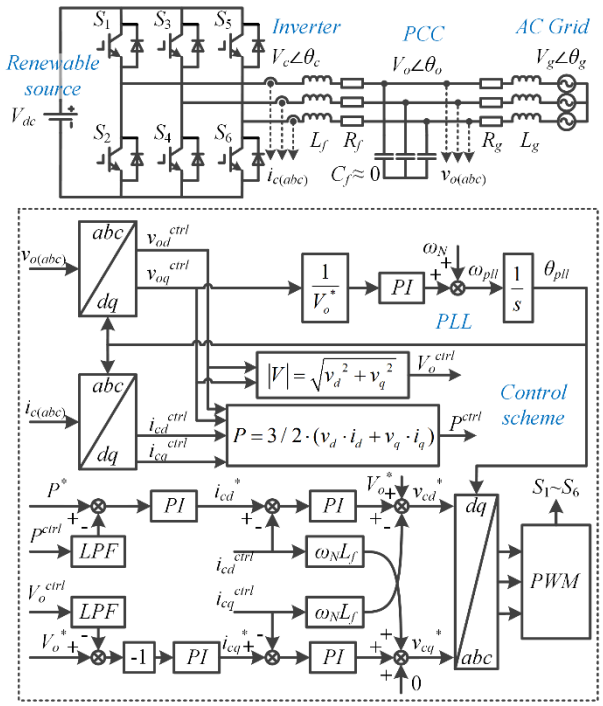

Fig. 1. Schematic diagram of classical VCC grid-following inverter.

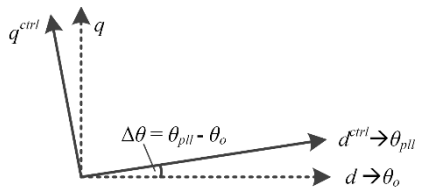

Fig. 2. Schematic diagram of voltage-oriented *d-q* frames.

The control system in Fig. 1 is performed in the rotating *d-q* frame, which is synchronized to the voltage phase angle at the PCC obtained by the PLL. Although the *d-q* control frame is expected to be oriented to the PCC voltage phase angle θ_o, the phase angle θ_o is unknown. So it is usually oriented to the PLL output angle θ_{pll}. These two angles have a small-signal error in the dynamic state [8]. Thus, the system *d-q* frame and the control *d-q* frame are shown in Fig. 2. The superscript '*ctrl*' denotes the variables in the control *d-q* frame.

In Fig. 1, $V_g\angle\theta_g$ is the grid voltage, $V_o\angle\theta_o$ is the output voltage at the PCC, and $V_c\angle\theta_c$ is the converter output voltage. $v_{o(abc)}$ and $i_{c(abc)}$ are instantaneous values of the PCC voltage and the converter current. The AC grid is represented by a Thevenin's equivalent impedance $Z_g = R_g + j\omega L_g$, where ω is the grid frequency, R_g and L_g are the equivalent grid resistance and inductance. As the AC grid in this paper is considered as an infinite grid, the grid angular frequency ω is constant and equal to its nominal value ω_N. C_f is the output filter capacitance. L_f and R_f are the output filter inductance and resistance. In order to avoid low-frequency passive resonances on the AC side, the value of C_f should be very small. The control diagram shown in Fig. 1 includes a *d*-axis inner current control loop, a *q*-axis inner current control loop, an outer active power control loop, an outer AC voltage amplitude control loop, and a PLL. The AC voltage amplitude reference is 1 per unit (pu), which means $V_o^* = V_g$. The definition of the SCR can be found in [2]. A very weak grid condition with SCR = 1 is used for all analyses in this paper.

B. Small-Signal Impedance Model

In order to analyze the stability of the nonlinear system, the small-signal linearized models are effective tools. Compared with other models, the impedance model is good at revealing the intrinsic relationship among variables, so it is used for analysis in this paper. In the following sections, the subscript '$_0$' denotes a steady-state operating point, and the symbol 'Δ' denotes a small-signal perturbation of a variable.

The small-signal linearized expressions of the physical circuits in the grid *d-q* frame are given by (1)-(3).

$$\begin{bmatrix}\Delta v_{od}\\ \Delta v_{oq}\end{bmatrix}-\begin{bmatrix}\Delta v_{gd}\\ \Delta v_{gq}\end{bmatrix}=\begin{bmatrix}sL_g+R_g & -\omega L_g\\ \omega L_g & sL_g+R_g\end{bmatrix}\cdot\begin{bmatrix}\Delta i_{od}\\ \Delta i_{oq}\end{bmatrix} \tag{1}$$

$$\begin{bmatrix}\Delta i_{cd}\\ \Delta i_{cq}\end{bmatrix}-\begin{bmatrix}\Delta i_{od}\\ \Delta i_{oq}\end{bmatrix}=\begin{bmatrix}sC_f & -\omega C_f\\ \omega C_f & sC_f\end{bmatrix}\cdot\begin{bmatrix}\Delta v_{od}\\ \Delta v_{oq}\end{bmatrix} \tag{2}$$

$$\begin{bmatrix}\Delta v_{cd}\\ \Delta v_{cq}\end{bmatrix}-\begin{bmatrix}\Delta v_{od}\\ \Delta v_{oq}\end{bmatrix}=\begin{bmatrix}sL_f+R_f & -\omega L_f\\ \omega L_f & sL_f+R_f\end{bmatrix}\cdot\begin{bmatrix}\Delta i_{cd}\\ \Delta i_{cq}\end{bmatrix} \tag{3}$$

The small-signal linearized expressions of the coordinate transformation between the grid *d-q* frame and the control *d-q* frame can be derived as:

$$\begin{bmatrix}\Delta v_{od}^{\ ctrl}\\ \Delta v_{oq}^{\ ctrl}\end{bmatrix}=\begin{bmatrix}\Delta v_{od}\\ \Delta v_{oq}\end{bmatrix}+\begin{bmatrix}v_{oq0}\\ -v_{od0}\end{bmatrix}\cdot\Delta\theta_{pll} \tag{4}$$

$$\begin{bmatrix}\Delta i_{cd}^{\ ctrl}\\ \Delta i_{cq}^{\ ctrl}\end{bmatrix}=\begin{bmatrix}\Delta i_{cd}\\ \Delta i_{cq}\end{bmatrix}+\begin{bmatrix}i_{cq0}\\ -i_{cd0}\end{bmatrix}\cdot\Delta\theta_{pll} \tag{5}$$

$$\begin{bmatrix}\Delta v_{cd}\\ \Delta v_{cq}\end{bmatrix}=\begin{bmatrix}\Delta v_{cd}^{\ ctrl}\\ \Delta v_{cq}^{\ ctrl}\end{bmatrix}+\begin{bmatrix}-v_{cq0}\\ v_{cd0}\end{bmatrix}\cdot\Delta\theta_{pll} \tag{6}$$

The small-signal linearized expression of the PLL in the control *d-q* frame can be derived as:

$$\Delta\theta_{pll}=(K_{p\_pll}+\frac{1}{s}\cdot K_{i\_pll})\cdot\frac{1}{sV_o}\cdot\Delta v_{oq}^{\ ctrl} \tag{7}$$

By substituting (4) into (7), the expression of $\Delta\theta_{pll}$ can be derived as:

$$\Delta\theta_{pll}=\frac{K_{p\_pll}s+K_{i\_pll}}{s^2+K_{p\_pll}s+K_{i\_pll}}\cdot\frac{1}{V_o}\cdot\Delta v_{oq}=\frac{G_{pll}}{V_o}\cdot\Delta v_{oq} \tag{8}$$

where $K_{p\_pll}=2\cdot\zeta\cdot\omega_n$, $K_{i\_pll}=\omega_n^2$, ζ is the damping ratio of the second-order system, and ω_n is the natural angular frequency of the second-order system, which is proportional to the bandwidth of the PLL if the damping ratio ζ is given.

By substituting (8) and "$v_{od0} = V_o$, $v_{oq0} = 0$" into (4), the expression of $\Delta v_{odq}^{\ ctrl}$ is deduced as:

$$\begin{bmatrix}\Delta v_{od}^{\ ctrl}\\ \Delta v_{oq}^{\ ctrl}\end{bmatrix}=\begin{bmatrix}\Delta v_{od}\\ \Delta v_{oq}\end{bmatrix}-\begin{bmatrix}0 & 0\\ 0 & G_{pll}\end{bmatrix}\cdot\begin{bmatrix}\Delta v_{od}\\ \Delta v_{oq}\end{bmatrix} \tag{9}$$

By substituting (8) into (5), the expression of $\Delta i_{cdq}{}^{ctrl}$ is deduced as:

$$\begin{bmatrix} \Delta i_{cd}{}^{ctrl} \\ \Delta i_{cq}{}^{ctrl} \end{bmatrix} = \begin{bmatrix} \Delta i_{cd} \\ \Delta i_{cq} \end{bmatrix} - \begin{bmatrix} 0 & \dfrac{-i_{cq0}}{V_o} \cdot G_{pll} \\ 0 & \dfrac{i_{cd0}}{V_o} \cdot G_{pll} \end{bmatrix} \cdot \begin{bmatrix} \Delta v_{od} \\ \Delta v_{oq} \end{bmatrix} \tag{10}$$

By substituting (8) into (6), the expression of Δv_{cdq} is deduced as:

$$\begin{bmatrix} \Delta v_{cd} \\ \Delta v_{cq} \end{bmatrix} = \begin{bmatrix} \Delta v_{cd}{}^{ctrl} \\ \Delta v_{cq}{}^{ctrl} \end{bmatrix} + \begin{bmatrix} 0 & \dfrac{-v_{cq0}}{V_o} \cdot G_{pll} \\ 0 & \dfrac{v_{cd0}}{V_o} \cdot G_{pll} \end{bmatrix} \cdot \begin{bmatrix} \Delta v_{od} \\ \Delta v_{oq} \end{bmatrix} \tag{11}$$

where the steady-state values v_{cdq0} can be expressed as: $v_{cd0} = v_{od0} + R_f i_{cd0} - \omega L_f i_{cq0}$, and $v_{cq0} = v_{oq0} + R_f i_{cq0} + \omega L_f i_{cd0}$.

Moreover, the small-signal linearized expression of the inner control loop is given by (12).

$$\begin{aligned} \begin{bmatrix} \Delta v_{cd}{}^{*} \\ \Delta v_{cq}{}^{*} \end{bmatrix} &= \begin{bmatrix} G_{pi\_I} & 0 \\ 0 & G_{pi\_I} \end{bmatrix} \cdot \left(\begin{bmatrix} \Delta i_{cd}{}^{*} \\ \Delta i_{cq}{}^{*} \end{bmatrix} - \begin{bmatrix} \Delta i_{cd}{}^{ctrl} \\ \Delta i_{cq}{}^{ctrl} \end{bmatrix} \right) \\ &+ \begin{bmatrix} 0 & -\omega L_f \\ \omega L_f & 0 \end{bmatrix} \cdot \begin{bmatrix} \Delta i_{cd}{}^{ctrl} \\ \Delta i_{cq}{}^{ctrl} \end{bmatrix} \end{aligned} \tag{12}$$

where $G_{pi\_I} = K_{p\_id} + K_{i\_id} / s = K_{p\_iq} + K_{i\_iq} / s$.

The small-signal linearized expressions of the outer control loops are given by (13).

$$\begin{bmatrix} \Delta i_{cd}{}^{*} \\ \Delta i_{cq}{}^{*} \end{bmatrix} = \begin{bmatrix} G_{pi\_P} & 0 \\ 0 & -G_{pi\_V} \end{bmatrix} \cdot \left(\begin{bmatrix} \Delta P^{*} \\ \Delta V_o{}^{*} \end{bmatrix} - \begin{bmatrix} \Delta P_{LPF}{}^{ctrl} \\ \Delta V_{oLPF}{}^{ctrl} \end{bmatrix} \right) \tag{13}$$

where $G_{pi\_P} = K_{p\_P} + K_{i\_P} / s$ and $G_{pi\_V} = K_{p\_V} + K_{i\_V} / s$.

Furthermore, the small-signal linearized expressions of the active power and the AC voltage amplitude feedbacks are shown as (14).

$$\begin{aligned} \begin{bmatrix} \Delta P^{ctrl} \\ \Delta V_o{}^{ctrl} \end{bmatrix} &= \begin{bmatrix} 3/2 \cdot i_{cd0} & 3/2 \cdot i_{cq0} \\ 1 & 0 \end{bmatrix} \cdot \begin{bmatrix} \Delta v_{od}{}^{ctrl} \\ \Delta v_{oq}{}^{ctrl} \end{bmatrix} \\ &+ \begin{bmatrix} 3/2 \cdot V_o & 0 \\ 0 & 0 \end{bmatrix} \cdot \begin{bmatrix} \Delta i_{cd}{}^{ctrl} \\ \Delta i_{cq}{}^{ctrl} \end{bmatrix} \end{aligned} \tag{14}$$

By choosing the same cut-off angular frequency of the first-order low-pass filters (LPFs) for the power and the voltage, the small-signal linearized expressions are shown as (15).

$$\begin{bmatrix} \Delta P_{LPF}{}^{ctrl} \\ \Delta V_{oLPF}{}^{ctrl} \end{bmatrix} = \begin{bmatrix} G_{LPF} & 0 \\ 0 & G_{LPF} \end{bmatrix} \cdot \begin{bmatrix} \Delta P^{ctrl} \\ \Delta V_o{}^{ctrl} \end{bmatrix} \tag{15}$$

where $G_{LPF} = \omega_{LPF} / (s + \omega_{LPF})$ and ω_{LPF} is the cut-off angular frequency of the first-order LPF.

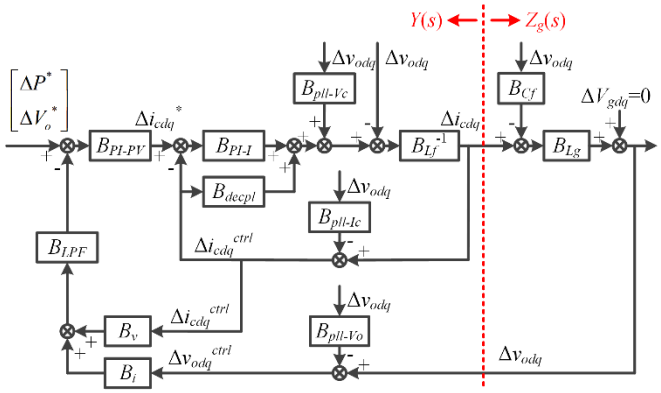

Fig. 3. Small-signal control structure of grid-following inverter.

Overall, the 2×2 matrixes in (1)-(3) can be represented by B_{Lg}, B_{Cf} and B_{Lf}. The 2×2 matrixes in (9)-(11) can be represented by $B_{pll\text{-}Vo}$, $B_{pll\text{-}Ic}$ and $B_{pll\text{-}Vc}$. The 2×2 matrixes in (12)-(13) can be represented by $B_{PI\text{-}I}$, B_{decpl} and $B_{PI\text{-}PV}$. And the 2×2 matrixes in (14)-(15) can be represented by B_i, B_v and B_{LPF}. Thus, the small-signal control structure of the system is shown in Fig. 3.

It is revealed in [13] that the small-signal control structure in Fig. 3 can be represented by a Norton-Thevenin equivalent model. And the equivalent admittance $Y(s)$ and impedance $Z_g(s)$ can be used for stability analysis.

Based on the control structure in Fig. 3, considering Δi_{cdq} as input and Δv_{odq} as output for the grid-side subsystem, the equivalent impedance $Z_g(s)$ can be given as (16). If the capacitance C_f is very small, B_{Cf} in (16) can be ignored.

$$Z_g(s) = (B_{Lg}{}^{-1} + B_{Cf})^{-1} \approx B_{Lg} \tag{16}$$

Similarly, considering Δv_{odq} as input and $-\Delta i_{cdq}$ as output for the converter-side subsystem, the equivalent admittance $Y(s)$ can be derived as (17).

$$\begin{aligned} Y(s) = &[B_{Lf} + B_{PI-I} - B_{decpl} + B_{PI-I} B_{PI-PV} B_{LPF} B_v]^{-1} \cdot \\ &[I - (B_{PI-I} - B_{decpl} + B_{PI-I} B_{PI-PV} B_{LPF} B_v) \cdot B_{pll-Ic} \\ &- B_{pll-Vc} + B_{PI-I} B_{PI-PV} B_{LPF} B_i \cdot (I - B_{pll-Vo})] \end{aligned} \tag{17}$$

Take $G_{pi\_I} = \omega_i L_f + \omega_i R_f / s$ for the current control loop, $G_{pi\_P} = \omega_p \cdot 1/(1.5 V_o) \cdot (1/\omega_{LPF} + 1/s)$ for the power control loop and $G_{pi\_V} = \omega_v \cdot I_{max} / V_o \cdot (1/\omega_{LPF} + 1/s)$ for the voltage control loop, where ω_i, ω_p and ω_v are the expected bandwidths of the current loop, the power loop, and the voltage loop. Then, the equivalent admittance $Y(s)$ in (17) can be derived as:

$$Y(s) = \begin{bmatrix} Y_{dd}(s) & Y_{dq}(s) \\ Y_{qd}(s) & Y_{qq}(s) \end{bmatrix} \tag{18}$$

where $Y_{dd}(s) = [s/(s\omega_i L_f + \omega_i R_f) + i_{cd0}\omega_p/(V_o s)] / [(s+\omega_i)/\omega_i + \omega_p/s]$, $Y_{dq}(s) = [G_{pll} i_{cq0}(s\omega_i L_f + \omega_i R_f + sR_f)/V_o/(s\omega_i L_f + \omega_i R_f) + i_{cq0}\omega_p/(V_o s)]/[(s+\omega_i)/\omega_i + \omega_p/s]$, $Y_{qd}(s) = (-I_{max}\omega_v\omega_i) / [V_o s(s+\omega_i)]$, and $Y_{qq}(s) = [(1-G_{pll})s - G_{pll} i_{cd0}(s\omega_i L_f + \omega_i R_f + sR_f)/V_o] / [(sL_f + R_f)(s+\omega_i)]$.

Thus, according to (16) and (18), the matrix $Y(s) \cdot Z_g(s)$ can be used by GNC for stability analysis [8], [13].

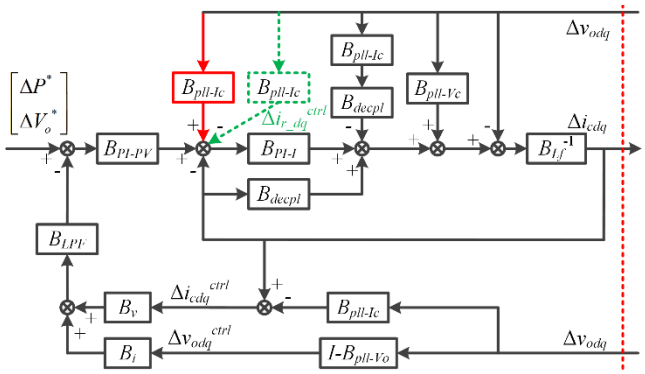

Fig. 4. Small-signal structure to make an expected reshaped impedance.

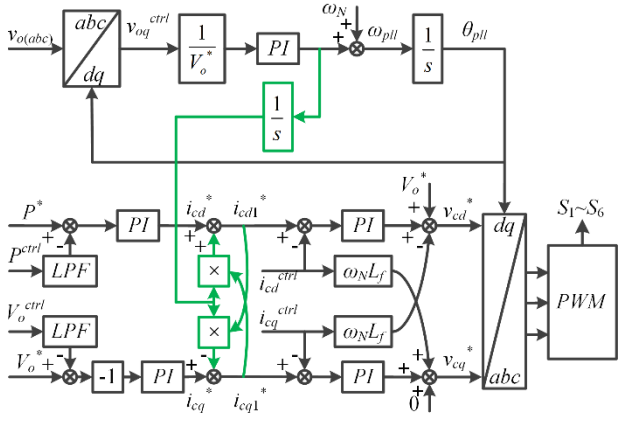

Fig. 5. Proposed improved grid-following control scheme based on Fig. 1.

III. Impedance Reshaping Method

In the previous section, the small-signal linearized model is established to analyze the control stability of the system. By connecting all the lines of Δv_{odq}, the converter-side subsystem in Fig. 3 can be shown as an equivalent structure in Fig. 4. Because the negative resistance in $Y_{qq}(s)$ causes positive feedback in the control loop, which is marked in red in Fig. 4, it is a major destabilizing factor. To counteract the positive feedback in the control loop, additional negative feedback is expected to be added, which is marked by green dotted line in Fig. 4.

According to Fig. 4, the current feedforward term from Δv_{odq}^{ctrl} to $\Delta i_{r\_dq}^{ctrl}$ is derived as:

$$\begin{bmatrix} \Delta i_{r\_d}^{ctrl} \\ \Delta i_{r\_q}^{ctrl} \end{bmatrix} = \frac{\Delta v_{oq}^{ctrl}}{V_o} \cdot \left(K_{p\_pll} + \frac{K_{i\_pll}}{s}\right) \cdot \frac{1}{s} \cdot \begin{bmatrix} -i_{cq0} \\ i_{cd0} \end{bmatrix} \tag{19}$$

The steady-state value i_{cdq0} in (19) can be represented by reference value in the control scheme. Thus, the implementation of the proposed improved control scheme is shown in Fig. 5.

Table I shows the system and control parameters. By using these parameters, the impedance characteristics of original $Y_{qq}(s)$ and reshaped $Y_{qq}(s)$ are compared in Fig. 6 when the active power P is 0.6 pu. It can be seen that the $Y_{qq}(s)$ is reshaped from negative resistance characteristic to the positive resistance characteristic within the frequency range [243 rad/s, 308 rad/s].

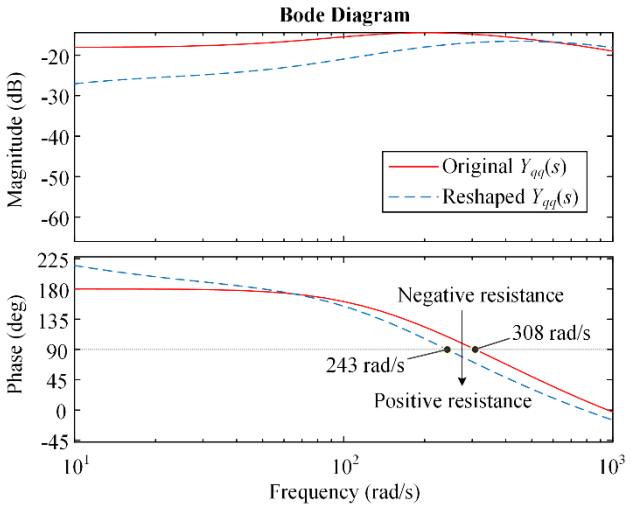

Fig. 6. Impedance characteristics of original $Y_{qq}(s)$ and reshaped $Y_{qq}(s)$ when SCR = 1 and P = 0.6 pu.

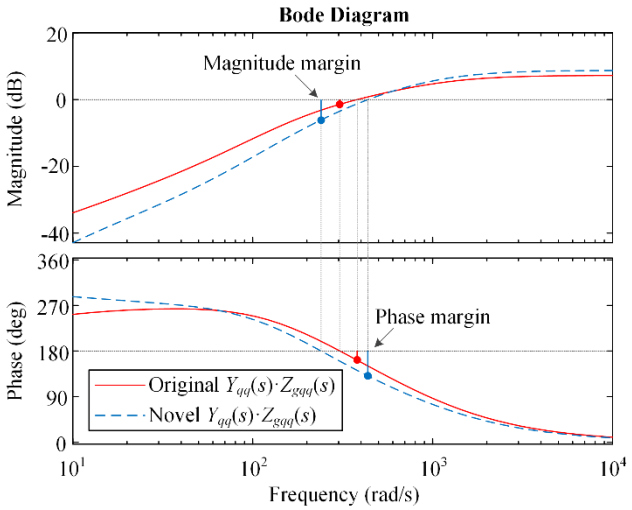

Fig. 7. Bode diagram of original $Y_{qq}(s)\cdot Z_{gqq}(s)$ and novel $Y_{qq}(s)\cdot Z_{gqq}(s)$ when SCR = 1 and P = 0.6 pu.

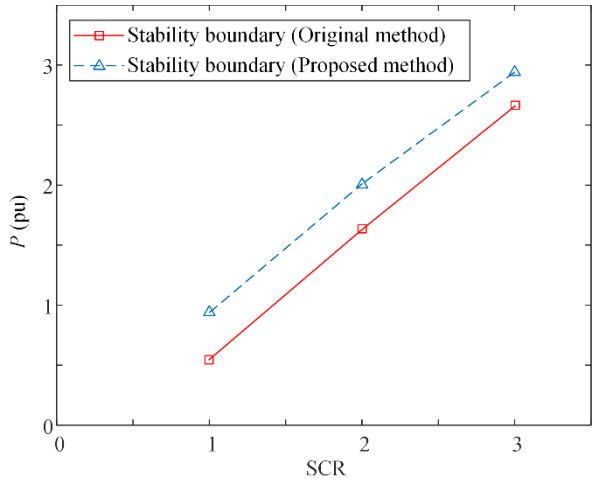

Fig. 8. Small-signal stability boundaries of classical control scheme and proposed control scheme in Fig. 5.

TABLE I. PARAMETERS OF GRID-FOLLOWING INVERTER

Parameters	Values
Grid phase voltage (peak value), V_g	311 V
Grid frequency, f_g	50 Hz
Rated power of inverter, S_N	30 kVA
Maximum current of inverter (peak value), I_{max}	64.3 A
DC-link voltage, V_{dc}	700 V
Output filter inductor, L_f	5 mH
Output filter capacitor, C_f	5 μF
R/X ratio of grid impedance, R_g/X_g	0.01
Short circuit ratio, SCR	1
Grid inductor, L_g	15.3 mH
Grid resistor, R_g	0.048 Ω
Sampling period, T_s	100 μs
Expected bandwidth of current loop, ω_i	1000 rad/s
Expected bandwidth of AC voltage loop, ω_v	50 rad/s
Expected bandwidth of active power loop, ω_p	10 rad/s
Cut-off angular frequency of LPF, ω_{LPF}	200 rad/s
Damping ratio of PLL, ζ	1
Natural angular frequency of PLL, ω_n	200 rad/s

According to the comparison of impedance characteristics in Fig. 6, the negative resistance in $Y_{qq}(s)$ can be reduced by using the proposed control scheme. Moreover, in order to see the impact on the stability by choosing different control schemes, the Bode diagrams of the original and novel $Y_{qq}(s)\cdot Z_g(s)$ are shown in Fig. 7. It can be seen clearly that the stability margin is improved by using the proposed method.

However, it is just an approximate method by using Bode diagram to analyze the stability of a multiple-input multiple-output (MIMO) system. To analyze the stability accurately for the MIMO system, the GNC should be used.

Based on GNC, the stability boundaries of the classical grid-following control scheme and the proposed improved grid-following control scheme are compared in Fig. 8, where the stability boundary means the maximum stable operating point of the active power. It can be seen that the stability boundary can be improved under different grid strength conditions. When SCR is equal to 1, the stability boundary is improved from 0.55 pu to 0.95 pu.

It is worth mentioning that because the inner current control loops are designed with very high bandwidths and the outer voltage and power control loops are designed with very low bandwidths, their impacts on the stability are not obvious. Thus, the small-signal stability of the system mainly depends on the PLL dynamics. In addition, decreasing the PLL bandwidth is an alternative way to reduce the negative resistance characteristic in $Y_{qq}(s)$ and enhance the stability, but the frequency dynamic response of the PLL is slow in this way [14].

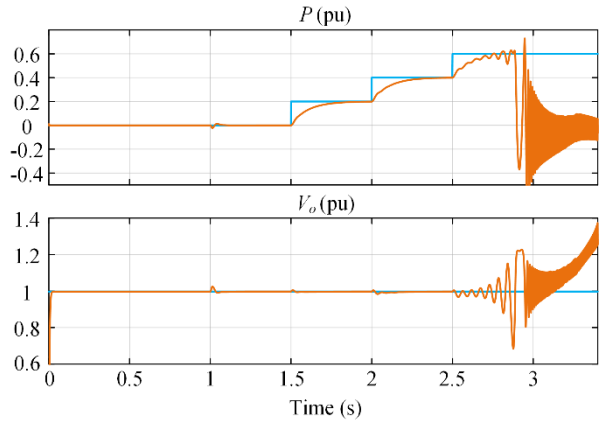

Fig. 9. Simulation results of classical control scheme with SCR=1.

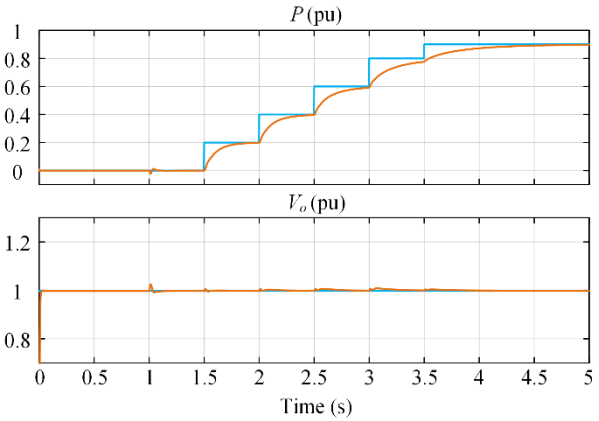

Fig. 10. Simulation results of proposed control scheme in Fig. 5 with SCR=1.

IV. SIMULATION RESULTS

In order to verify the effectiveness of the proposed method, a time-domain simulation model of a 30 kVA grid-connected inverter is built in Matlab/Simulink. To avoid the influence of high-frequency harmonics, an average model of the inverter is used. The system and control parameters are the same with Table I. Given 0.6 pu power reference for the classical control scheme and 0.9 pu power reference for the proposed control scheme, the simulation results are shown in Fig. 9 and Fig. 10 respectively.

As seen in Fig. 9, when the power reference is lower than 0.4 pu, the system is stable by using the classical control scheme. However, the PCC voltage starts to oscillate when the power reference is close to 0.6 pu. Finally, the system becomes unstable and both the PCC voltage and the active power are out of control.

Differently, as seen in Fig. 10, when the power reference is lower than 0.9 pu, the system is always stable by using the proposed control scheme in Fig. 5. The simulation results shown in Fig. 9 and Fig. 10 agree well with the estimated results by small-signal stability analysis in Fig. 8.

It is worth mentioning that although the proposed control method can enhance the stability of the system, it only works under the ideal condition that the grid angular frequency ω is

constant and always equal to its nominal value ω_N. However, when the grid angular frequency ω is different from ω_N, the proposed method cannot work. How to solve this problem will become our future research direction.

V. Conclusions

This paper reveals that the positive feedback caused by the PLL is a major destabilizing factor for the classical grid-following control scheme. To solve this problem, a novel impedance reshaping method is proposed, which can enhance the stability and extend the stability range. Simulation results verify the effectiveness of the proposed method.

References

[1] F. Blaabjerg, Y. Yang, D. Yang, and X. Wang, "Distributed power generation systems and protection," *Proc. IEEE*, vol. 105, no. 7, pp. 1311-1331, Jul. 2017.

[2] D. Yang, X. Wang, F. Liu, K. Xin, Y. Liu, et al., "Adaptive reactive power control of PV power plants for improved power transfer capability under ultra-weak grid conditions," *IEEE Trans. Smart Grid*, vol. 10, no. 2, pp. 1269-1279, Mar. 2019.

[3] J. A. Suul, S. D'Arco, P. Rodriguez, and M. Molinas, "Impedance-compensated grid synchronization for extending the stability range of weak grids with voltage source converters," *IET Gener., Trans. Distr.*, vol. 10, no. 6, pp. 1315-1326, Apr. 2016.

[4] X. Wang, M. G. Taul, H. Wu, Y. Liao, F. Blaabjerg, et al, "Grid-synchronization stability of converter-based resources – an overview," *IEEE Open J. Ind. Appl.*, vol. 1, pp. 115-134, Aug. 2020.

[5] K. M. Cheema, "A comprehensive review of virtual synchronous generator," *Electrical Power Energy Syst.*, vol. 120, pp. 1-10, 2020.

[6] A. Egea-Alvarez, S. Fekriasl, F. Hassan, and O. Gomis-Bellmunt, "Advanced vector control for voltage source converters connected to weak grids," *IEEE Trans. Power Syst.*, vol. 30, pp. 3072-3081, 2015.

[7] K. Givaki, D. Chen, and L. Xu, "Current error based compensation for VSC current control in weak grids for wind farm applications," *IEEE Trans. Sustain. Energy*, vol. 10, no. 1, pp. 26-35, Jan. 2019.

[8] B. Wen, D. Boroyevich, R. Burgos, P. Mattavelli, and Z. Shen, "Analysis of D-Q small-signal impedance of grid-tied inverters," *IEEE Trans. Power Electron.*, vol. 31, no. 1, pp. 675-687, Jan. 2016.

[9] J. Fang, X. Li, H. Li, and Y. Tang, "Stability improvement for three-phase grid-connected converters through impedance reshaping in quadrature-axis," *IEEE Trans. Power Electron.*, vol. 33, no. 10, pp. 8365-8375, Oct. 2018.

[10] D. Yang, X. Wang, F. Liu, K. Xin, Y. Liu, et al, "Symmetrical PLL for SISO impedance modeling and enhanced stability in weak grids," *IEEE Trans. Power Electron.*, vol. 35, no. 2, pp. 1473-1483, Feb. 2020.

[11] K. M. Alawasa, Y. A. I. Mohamed, and W. Xu, "Active mitigation of subsynchronous interactions between PWM voltage-source converters and power networks," *IEEE Trans. Power Electron.*, vol. 29, no. 1, pp. 121-134, Jan. 2014.

[12] J. I. Garcia, J. I. Candela, and P. Catalan, "Pre-filtered synchronization structure for grid-connected power converters to reduce the stability impact of PLL dynamics," *IEEE J. Emerg. Select. Topics Power Electron., (Early Access)*, Sep. 2020.

[13] J. F. Morris, K. H. Ahmed, and A. Egea-Alvarez, "Analysis of controller bandwidth interactions for vector-controlled VSC connected to very weak AC grids," *IEEE J. Emerg. Select. Topics Power Electron., (Early Access)*, Oct. 2020.

[14] A. A. Nazib, D. G. Holmes, and B. P. McGrath, "Decoupled DSOGI-PLL for improved three phase grid synchronisation," *IEEE Int. Power Electron. Conf.*, Niigata, Japan, pp. 3670-3677, 2018.